Scientific Research Publishing

Atmospheric and Climate Sciences, 2025, 15(4), 723-741
https://www.scirp.org/journal/acs
ISSN Online: 2160-0422
ISSN Print: 2160-0414

Long Term Characterization of Dust and Its Radiative Forcing over Kenya Using Satellite and Model-Based Data

Kizito W. Simiyu, Geoffrey W. Khamala, John W. Makokha

Department of Science Technology and Engineering, Kibabii University, Bungoma, Kenya
Email: makokhajw@kibu.ac.ke

How to cite this paper: Simiyu, K.W., Khamala, G.W. and Makokha, J.W. (2025) Long Term Characterization of Dust and Its Radiative Forcing over Kenya Using Satellite and Model-Based Data. *Atmospheric and Climate Sciences*, **15**, 723-741.
https://doi.org/10.4236/acs.2025.154037

Received: July 2, 2025
Accepted: August 30, 2025
Published: September 2, 2025

Abstract

Dust aerosols play a critical role in atmospheric processes, influencing air quality, climate, and weather patterns through their interactions with radiation and cloud formation. This study aimed at characterizing the spatiotemporal distribution of dust and quantifying its radiative forcing over Kenya using a combination of satellite observations and model-based measurements. Multi-year datasets from MERRA-2 and MODIS were utilized to analyze dust loading and spatial variability. Additionally, radiative forcing (RF) derived from MERRA-2 and satellite observations was estimated to assess dust-induced changes in surface of-atmosphere (BOA), top-of-atmosphere (TOA) and within atmosphere (ATM). The findings on spatiotemporal variability of dust over Kenya, highlight high concentrations in northern regions during dry months and reductions during wet seasons (MAM and OND). While on particle size distribution, the analysis shows coarse-mode dominance in dry periods, depicting dominance of dust. On the other hand, dust mass concentrations peak in the northwest part of the study domain. Further, RF analysis indicates dust induces BOA and TOA cooling but atmospheric heating, with peak heating in June to July, local dry months. This study therefore recommends an enhanced integrated dust monitoring and modeling system, especially during dry seasons, to capture Dust AOD, size, and mass concentration. Further, targeted mitigation measures like afforestation, land-use planning and early warning systems should be prioritized to reduce dust emissions, improve climate model accuracy, and protect public health in vulnerable regions.

Keywords

Characterization, Dust, AOD, Radiative Forcing, Size Distribution

1. Introduction

Atmospheric aerosols are among the major drivers of climate forcing agents that are globally recognized [1] [2]. These aerosols, comprising fine solid particles or liquid droplets suspended in the atmosphere, play a pivotal role in Earth's climate system [3]-[5]. Further, they are emitted into the atmosphere either through natural or anthropogenic means [5] [6] and they significantly contribute to regional and global climate change. The total aerosol load consists of various aerosol species with dust originating from arid and semi-arid regions as the major aerosol contributor to the global aerosol load. As a fact, therefore, they have profound implications for radiative forcing and atmospheric dynamics [1] [2] [7]-[9]. Aerosols and majorly dust, affect climate directly by scattering and absorbing solar radiation, thereby modifying the radiation budget at the top, bottom, and within the atmosphere, which in turn influences the atmospheric heating rate [10]-[13]. The atmospheric heating rate is strongly dependent on aerosol optical depth (AOD) and single scattering albedo (SSA), being the column-integrated quantities that measure aerosol light extinction and absorption, respectively [14] [15]. In regions like Kenya, where local and transboundary dust sources converge, understanding the spatiotemporal variability and radiative impacts of mineral dust is essential for effective climate modeling [16].

The radiative effects of dust are multifaceted, including both direct and indirect interactions with solar and terrestrial radiation [17]-[28]. Dust particles scatter and absorb sunlight, modulating the atmospheric energy budget and influencing surface temperature [29]-[31]. These effects vary depending on the chemical composition, particle size distribution and optical properties of the dust [32]. Furthermore, dust aerosols act as cloud condensation nuclei (CCN) and ice-nucleating particles (INPs), altering cloud properties and precipitation patterns [33]. Over Kenya, the radiative forcing of mineral dust plays a significant role in shaping regional weather and climate patterns.

Advancements in model-based measurements and remote sensing technologies have revolutionized the study of dust. Numerical models, such as the Modern-Era Retrospective Analysis for Research and Applications, Version 2 (MERRA-2) [26] [33] [34] and satellite datasets from instruments like the Moderate Resolution Imaging Spectroradiometer (MODIS) [35] and the Cloud-Aerosol Lidar and Infrared Pathfinder Satellite Observation (CALIPSO), provide high-resolution data on aerosol properties. These tools enable comprehensive assessments of dust's spatial distribution and radiative impacts [27] [36].

Over the years, researchers have explored the dynamics of dust in various contexts, offering insights into its sources, transport mechanisms and interactions with atmospheric processes [16] [37]-[42]. For instance, [31] investigated global distribution and size variability of desert dust aerosols and highlighted that particle size influences the transport and deposition of dust, which in turn affects climate systems and nutrient cycles. In another related study, [37] delved into the physics of windblown sand and dust, and revealed that surface wind speeds, soil

properties, and vegetation coverage determine the intensity of dust events. Regionally, a study by [43] examined air pollution trends in East Africa from 2001 to 2021, identifying heterogeneous patterns with increasing pollution in certain hotspots and decreasing levels in other areas. Further, [44] focused on inhalable particulate matter in Uganda and found that both urban and rural areas experience significant levels of particulates, with urban areas like Kampala showing higher concentrations. While over the current study domain, [45] assessed changes in aerosol optical properties over Kenya during the COVID-19 lockdown period and reported insignificant effects on AOD spatial distributions.

Also, studies have been conducted over varied study domains on spatio-temporal radiative forcing. For instance, [12] conducted research on aerosol radiative forcing, emphasizing the role of dust in modulating atmospheric heating and surface cooling. While [46] focused on Middle East, investigating how dust alters atmospheric circulation and heating and reported a positive role of dust in modulating monsoon systems. On regional scale, [27] analyzed absorbing aerosols and their radiative forcing over various East African stations from 2001 to 2018 using AERONET and MERRA-2 and reported a spatio-temporal DARF at TOA, BOA and within the atmosphere. Therefore, the present study has analyzed the spatio-temporal characteristics of dust and quantified its radiative forcing over Kenya using satellite- and model-based measurements. The rest of this paper is structured as follows: the study area and meteorology section illustrate the study area, data, and methodology. Results and discussions are documented in the results and discussion section, while the conclusions and recommendation section summarizes the key findings drawn from the present work and call future research works to be undertaken.

2. Materials and Methods

2.1. Study Domain and Meteorology

The study domain covers located between latitudes 5˚S to 5˚N and longitudes 34˚E to 42˚E [45] and spans an area of 582,646 km^2 as depicted in **Figure 1**. It is bordered by Uganda to the west, Somalia to the east, Ethiopia to the north, Tanzania to the south and South Sudan to the northwest. It has a land area of about 569,137 km^2 with great diversity of landforms ranging from glaciated mountain peaks with permanent snow cover, through a flight of plateaus to the coastal plain [46]. Climatologically, Kenya has mostly tropical climate, with four distinct seasons based on rainfall patterns [47]. The wet seasons, March-April-May (MAM) and October-November-December (OND), are associated with lower AOD due to enhanced wet scavenging and reduced anthropogenic emissions. Conversely, the dry seasons, January-February (JF) and June-July-August-September (JJAS), exhibit higher AOD, driven by meteorological changes and increased emission sources [48] [49]. It has a distinct bimodal rainfall pattern which is influenced by the Inter Tropical Convergence Zone (ITCZ), global oceans, the tropical high pressure systems, tropical monsoons and tropical cyclones [5] [27]. This study

encompasses long term characterization of dust and its radiative forcing over Kenya using an integrated approach that combines satellite-based measurements and model simulations. Additionally, the research examines the radiative forcing of dust to assess its contribution to the Earth's energy budget and its role in influencing local and regional climate systems.

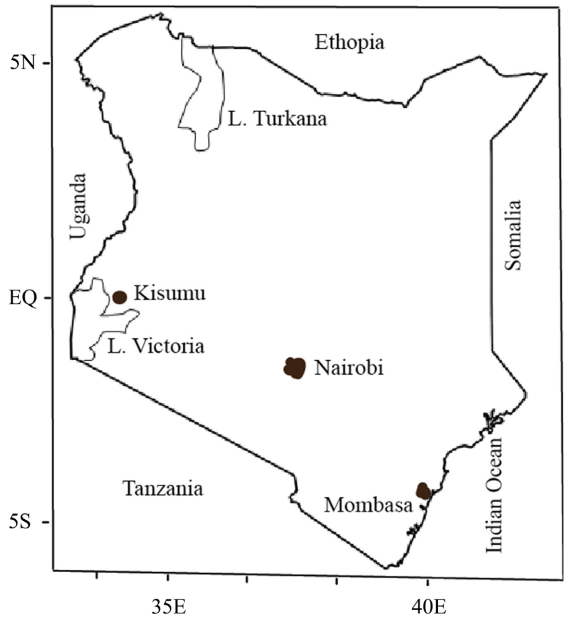

Figure 1. Geographical map of Kenya showing the locations of major cities, including Nairobi, Mombasa, and Kisumu. The map also highlights key water bodies such as Lake Victoria and Lake Turkana. The map is overlaid with latitude and longitude coordinates for spatial reference.

2.2. Instrumentation and Data

To conduct an effective spatio-temporal dust analysis, a combination of both satellite-derived and model-based measurements was used. Satellite data from MODIS, provide critical parameters such as aerosol optical depth (AOD) and dust retrievals [50]. It was launched into the Earth's orbit, with daytime equator crossing at 10:30 h local time (LT = UTC + 3h), by the National Aeronautics and Space Administration (NASA) Goddard Space Flight Center (GSFC) on 18th, December 1999 onboard the Terra satellite. The second was launched on May 4, 2002, onboard the Aqua platform [35] and has a daytime equator crossing at 13:30 h LT. The sensor has a swath of ~2330 km, with a temporal resolution of 1 - 2 days, and acquires data over 36 spectral bands ranging in wavelengths from 0.415 to 14.235 μm at three spatial resolutions (2 bands at 250 m, 5 bands at 500 m, and 29 bands at 1 km). Seven of these bands operating in near-ultraviolet (UV), visible and near infrared spectroscopy (IR) wavelength regions (0.415 - 2.155 μm) can effectively retrieve AOD over land and ocean [51]-[53] using two different algorithms: "Dark Target (DT)" and "Deep Blue (DB)". MODIS aerosol products are stored at different levels and under various versions called "collections." The MODIS data

processing levels include level 1.0 (geolocated radiance and brightness temperature), level 2.0 (retrieved geophysical data products), and level 3.0 (gridded points). MODIS retrieval accuracy over land and ocean [35] was estimated to be ±0.05 ± 0.20 (AOD) and ±0.03 ± 0.15 (AOD), respectively, for level 2 products. Detailed information concerning the sensor, data products, retrieval algorithms, calibration, and uncertainties can be found elsewhere [51] [52] [54].

On the other hand, MERRA-2 is a global atmospheric reanalysis dataset developed by NASA's Global Modeling and Assimilation Office (GMAO) and launched in 2009 [34]. It is based on the GEOS-5 atmospheric model, covering the period from 1980 to 2016 with a spatial resolution of 0.5˚ × 0.625˚ and 72 vertical layers, spanning the satellite observing era from 1980 to the present [26] [33] [34]. In 2017, the initial MERRA model was enhanced with improved analysis, forecasting, data assimilation, and bias correction of aircraft observations, leading to the development of MERRA-2 [36]. This model integrates meteorological data assimilation, aerosol analysis, precipitation, water vapor climatology, and temperature estimates using NASA's stratospheric ozone observations. Building on the success of GEOS-based reanalysis, MERRA-2 aims to provide a comprehensive Earth system reanalysis of the atmosphere, land, ocean, and ice. In this study, MERRA-2 M2TMNXAER v5.12.4 level-3 monthly time-averaged data were used to analyze trends in dust aerosols, which represent the total absorption and scattering per unit atmospheric depth. These datasets were sourced from http://giovanni.gsfc.nasa.gov/giovanni/.

2.3. Methodology

A number of key aerosol properties were analyzed to characterize dust load and optical effects. Dust AOD, a fundamental parameter representing columnar aerosol loading, was computed using Equation (1) that has been used by previous studies [55]:

$$\mathrm{AOD}_{\lambda} = \int_{Z_0}^{Z_1} \beta_{\lambda}(z)\,\mathrm{d}z \tag{1}$$

where $\beta_{\lambda}(z)$ is the extinction coefficient at altitude z and wavelength λ [35]. The Ångström exponent (AE) was also calculated to infer particle size, given by Equation (2) as:

$$\mathrm{AE} = \frac{\log\left(\mathrm{AOD}_{\lambda_1}/\mathrm{AOD}_{\lambda_2}\right)}{\log\left(\dfrac{\lambda_1}{\lambda_2}\right)} \tag{2}$$

where λ_1 and λ_2 are reference wavelengths. Low AE values (AE < 1) indicate coarse-mode aerosols such as dust, while higher values suggest fine-mode aerosols like smoke or urban pollution [56].

To estimate the mass concentration (μg/m^3) of dust aerosols, the following relationship in Equation (3) was employed:

$$M = \frac{\rho \mathrm{AOD}_{\lambda}}{Q_{ext} r_{eff}} \tag{3}$$

where ρ is the particle density, Q_{ext} the extinction efficiency and r_{eff} the effective radius [57]. On radiative forcing is connected via linear connection to global mean equilibrium temperature variation as given by Equation (4)

$$\Delta T_s = \Lambda RF \tag{4}$$

Atmospheric aerosols perturb the incoming shortwave and outgoing longwave radiation through the process known as direct aerosol radiative forcing (DARF). The DARF ($W \cdot m^{-2}$) at the bottom (BOA; 1 km) and top of the atmosphere (TOA; 100 km) is calculated as the change in the net fluxes with (F_{net}^{a}) and without (F_{net}^{b}) aerosols [23] [27].

$$\Delta F_{\text{BOA}} = F_{\text{net,BOA}}^{a} - F_{\text{net,BOA}}^{b} \tag{5}$$

$$\Delta F_{\text{TOA}} = F_{\text{net,TOA}}^{a} - F_{\text{net,TOA}}^{b} \tag{6}$$

Since the net flux (F_{net}) is the difference between the downward ($F_{\downarrow}$) and upward ($F_{\uparrow}$) fluxes, the radiative forcing at BOA and TOA was calculated using Equation (7) and Equation (8)

$$\Delta F_{\text{BOA}} = \left(F_{\downarrow,\text{BOA}}^{a} - F_{\uparrow,\text{BOA}}^{a}\right) - \left(F_{\downarrow,\text{BOA}}^{b} - F_{\uparrow,\text{BOA}}^{b}\right) \tag{7}$$

$$\Delta F_{\text{TOA}} = \left(F_{\downarrow,\text{TOA}}^{a} - F_{\uparrow,\text{TOA}}^{a}\right) - \left(F_{\downarrow,\text{TOA}}^{b} - F_{\uparrow,\text{TOA}}^{b}\right) \tag{8}$$

where ΔF is DARF while F^{b} and F^{b} are global irradiances with and without aerosols measured the TOA (ΔF_{TOA}) or BOA (ΔF_{BOA}), respectively. The net atmospheric forcing (ΔF_{ATM}), representing the amount of solar energy trapped in the atmosphere due to dust aerosols was calculated as the difference between dust TOA and BOA forcing (Equation (9)).

$$\Delta F_{\text{ATM}} = \Delta F_{\text{TOA}} - \Delta F_{\text{BOA}} \tag{9}$$

However, since MERRA-2 reports total aerosol radiative effects, this study isolated dust-only RF using dust-specific AOD (DUEXTTAU for total dust AOD) and then calculated RF due to dust using Equation (10)

$$\text{RF}_{\text{dust}} = \text{RF}_{\text{Total}} \times \frac{\text{AOD}_{\text{Dust}}}{\text{AOD}_{\text{Total}}} \tag{10}$$

where RF_{Total} MERRA-2 radiative forcing for all aerosols, $\frac{\text{AOD}_{\text{Dust}}}{\text{AOD}_{\text{Total}}}$ is the aerosol mixing ration for Dust specific AOD (AOD_{Dust}) and total aerosol AOD ($\text{AOD}_{\text{Total}}$). To achieve this, MERRA-2 data, including total aerosol radiative forcing and AOD dust components, were retrieved. The dust-specific monthly radiative forcing was then computed using Equation (10).

3. Results and Discussions

3.1. Spatiotemporal Analysis of Optical and Physical Properties of Dust

3.1.1. Spatial Analysis of Dust

The monthly dust variation over Kenya, as illustrated in **Figure 2**, exhibits a clear

seasonal pattern influenced by regional climatic conditions, wind regimes, rainfall distribution and surface characteristics. The spatial gradient of dust AOD consistently shows higher values in the northern and northeastern parts of the country, with the southern and central regions experiencing relatively lower levels throughout the year.

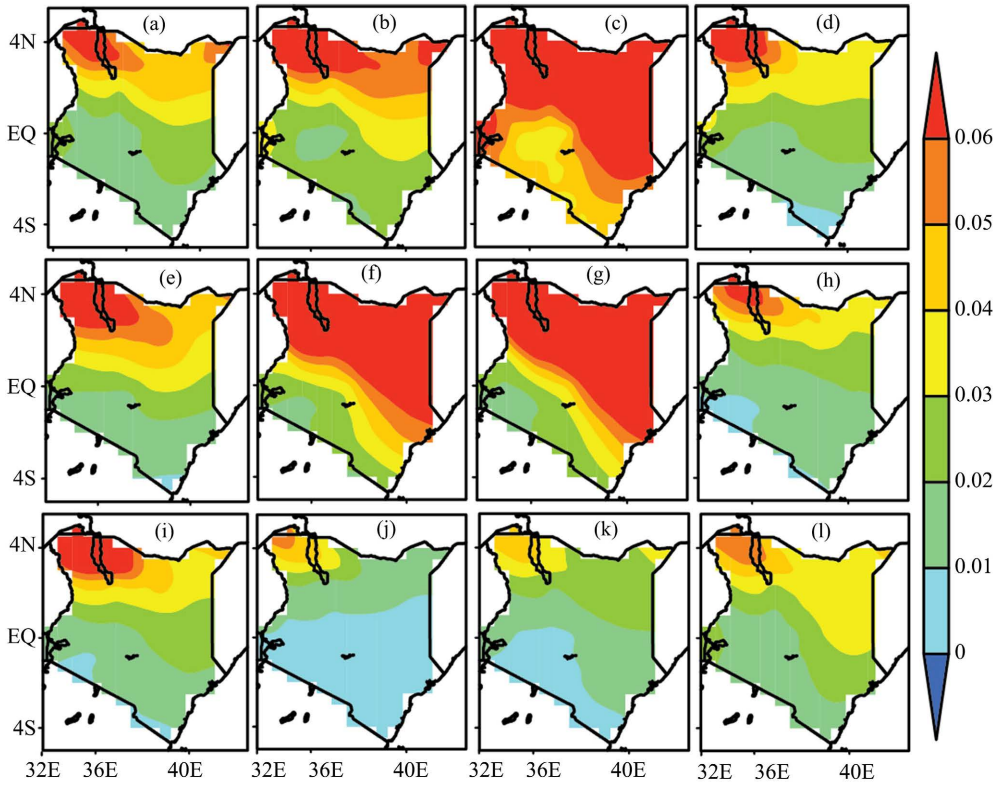

Figure 2. (a-l) Monthly distribution of dust AOD over Kenya (January-December). The figure illustrates the spatial and temporal trends of dust mass concentration across Kenya for each month of the year. The color bar indicates the intensity of dust loading.

From January to March, Kenya experiences its highest dust concentrations, particularly in the northern part of the domain [46]. This period corresponds to the dry season, during which rainfall is minimal or absent across most parts of the country. The arid and semi-arid landscapes of northern Kenya become major dust sources due to the dry, loose soil and sparse vegetation.

Additionally, the region is under the influence of the northeasterly (Harmattan) winds, which blow from the Arabian Peninsula and the Horn of Africa. These winds are dry and strong, favoring the uplift and transport of dust particles across the region. The intensity of the dust increases southwards into the central parts of Kenya but weakens before reaching the southern boundary, where vegetation cover and occasional rainfall offer some protection against dust emission.

In April, a noticeable decline in dust concentration begins. This marks the onset of the long rainy season (March to May) in many parts of Kenya. The increasing rainfall plays a critical role in suppressing dust activity by wetting the soil and

facilitating vegetation growth. Moist surfaces significantly reduce the availability of loose particles for wind erosion. This downward trend in dust levels continues through May, as rainfall becomes more widespread and persistent, especially over the highlands and central regions of the country. The reduction in wind speed and increased atmospheric moisture further inhibits dust emission [5] [27].

Between June and August, dust concentrations remain low across most parts of the study domain. The study domain during these months shows predominantly low dust concentration, indicating a relatively clean atmosphere in terms of dust. Although the northern parts of Kenya remain drier than the south, the cumulative effects of the previous rains and increased vegetation cover continue to restrain dust mobilization [58]. Moreover, cooler temperatures during this period help retain soil moisture and limit convective activities that might otherwise stir dust into the atmosphere [58] [59].

The months of September to November represent the period with the lowest dust concentrations across Kenya. These months coincide with a transitional climatic phase and the onset of the short rains season (typically October to December). While the short rains are not as intense or prolonged as the long rains, they are sufficient to maintain relatively moist surface conditions and moderate wind speeds [59] [60]. This combination minimizes the likelihood of dust uplift. Throughout this period, the entire study region, including the typically dusty north, exhibits the lowest dust loadings of the year.

In December, a resurgence in dust levels is observed, particularly in the northern regions, attributed to the gradual cessation of the short rains and the re-emergence of dry conditions [46]. As the soil dries out and vegetation begins to thin, the surface becomes more vulnerable to wind erosion once again. The northeasterly winds start to pick up strength towards the end of the month, contributing to the initial buildup of dust that will culminate in the peak season beginning in January.

3.1.2. Temporal Analysis of Dust

The temporal analysis of AOD_{Dust} over the study domain marked seasonal variability in atmospheric dust loading, with monthly variations reflecting the influence of meteorological conditions, land surface dynamics, and aerosol transport processes. The results have been tabulated in **Table 1**.

Dust levels are observed to be highest during the dry months, particularly in June and July, with mean AOD_{Dust} values of 0.0797 and 0.0657, respectively. These elevated values are attributed to enhanced surface wind activity, dry soil conditions, and reduced vegetation cover, all of which contribute to increased dust uplift and atmospheric loading [27] [59]. While June exhibits a slight positive trend in dust levels over the years, the month of July shows a notable declining trend in dust extinction, suggesting a possible reduction in dust emissions due to evolving land use practices, soil stabilization or regional climate changes. However, the correlation values (r^2) for these trends remain low, indicating that the changes are not strongly consistent over time. The JF season presents moderately

high dust values, with February peaking at 0.0516. Despite the relatively elevated dust levels, this period shows a general decline in dust loading, most pronounced in February, which records a substantial negative trend. The weakening of the Harmattan influence and the approach of the long rain season may be attributable to this decline.

Table 1. Monthly Mean Dust Extinction AOD_{550nm} 550 nm with the associated trends and correlation coefficient (r^2) indicating temporal variability in dust loading.

Months	Trends in Average Dust Extinction AOT 550 nm		
	Mean AOD_{Dust}	Trends (10^{-4})	r^2
January	0.0414	3.9484 ± 0.0003	0.0027
February	0.0516	−5.506 ± 0.0005	−0.2044
March	0.0509	−1.400 ± 0.0004	−0.5337
April	0.0298	−4.137 ± 0.0002	−0.4315
May	0.0311	−2.784 ± 0.0003	−0.1886
June	0.0797	1.836 ± 0.0008	0.0480
July	0.0657	−8.873 ± 0.0007	−0.2644
August	0.0329	−5.939± 0.0003	−0.3385
September	0.0247	−4.860 ± 0.0002	−0.5184
October	0.0185	−3.583 ± 0.0002	−0.4114
November	0.0250	−1.867 ± 0.0002	−0.2084
December	0.0333	−0.1346 ± 0.0003	−0.0102

On the other hand, during the long rain season (MAM), dust extinction values drop significantly from 0.0509 (March) to 0.0311 (May). This reduction is linked to wet deposition processes, where rainfall efficiently removes dust particles from the atmosphere and to increased vegetation cover, which reduces dust source availability [5] [9] [27] [59]. The consistent negative trends observed in wet months support the hypothesis that dust concentrations are generally decreasing during this season, likely due to interannual climatic variations and possibly improved land cover management.

In the latter part of the year, especially from August through November, the dust values remain relatively low, ranging from 0.0250 to 0.0333. This period also features strong negative trends, particularly in August and September, which may be associated with the transition from dry to wet conditions and a corresponding decline in dust mobilization. September records one of the lowest mean dust levels (0.0247) and a significantly negative trend, which may indicate sustained suppression of dust events during this period. The month of October, a local wet month, has the lowest dust extinction value (0.0185), further reinforces this seasonal decline. Finally, December exhibits a slight rebound in dust levels (0.0333), but the trend is nearly flat, indicating relative stability in dust concentrations during the

month, likely due to balanced meteorological and surface conditions that neither favor nor inhibit dust transport.

3.1.3. Particle Size Analysis of Dust

The monthly distribution of aerosol size over Kenya represented in Figure 3, shows a clear seasonal pattern that distinguishes between fine-mode aerosols and coarse-mode aerosols such as dust. To start with, in January (Figure 3(a)), the AE values are generally low ($0.5 < AE < 0.7$) across most parts of the study domain, except in the western regions, indicating a predominance of mixed particles (fine and coarse particles; Khamala *et al.*, 2023). The northern and northeastern regions show lower AE values (<0.5), suggesting the influence of coarse particles, possibly early signs of dust intrusion from adjacent arid zones.

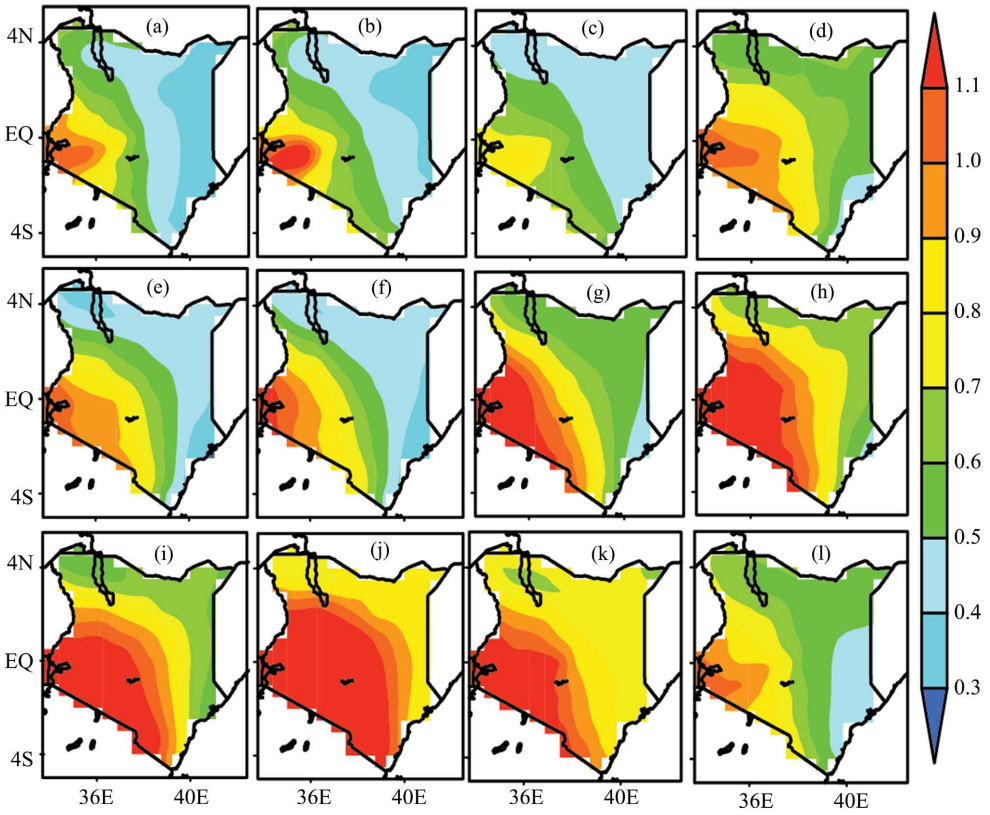

Figure 3. Monthly spatial variation of aerosol size over Kenya. Panels (a) to (l) represent the average aerosol particle size distribution from January to December, respectively. The color gradient reflects the mean aerosol size over the study domain.

As the season progresses into February and March (Figure 3(b) and Figure 3(c)), mixed aerosol-mode aerosols remain dominant in the central and southern regions, while coarser aerosols become more prominent in the north and east, depicted by decreasing AE values in those regions (>0.5). This gradual transition reflects increasing dust uplift in drier areas. During the long rains, April (Figure 3(d)) generally corresponds with higher AE values (>0.5) over most parts of the domain, indicating fine aerosol conditions as rainfall suppresses dust emissions

and promotes wet scavenging. However, Eastern Kenya maintains slightly lower AE values ($0.5 < AE < 0.6$), hinting at persistent dust presence.

From May through August (**Figures 3(e)-(h)**), the domain enters the peak in the fine mode aerosols, especially in western and central regions. This is clearly indicated by high AE values ($AE > 1.1$), which reflect the dominance of fine-mode particles. The Southern Africa experiences intense biomass burning (forest and savanna fires) during the JJAS season, releasing large quantities of fine-mode aerosols (e.g., organic carbon, black carbon). Due to prevailing southerly and southeasterly winds, these plumes are transported northward across the equator, often reaching eastern and central Kenya.

During the months of September, October and November (**Figures 3(i)-(k)**), dust concentrations over Kenya show a progressive decline, particularly as the country transitions from the dry season to the onset of the short rains, depicted in increasing AE. In September, some residual dust remains, especially over the northern and northeastern arid regions, such as Turkana, Marsabit, and Wajir**,** where vegetation is still sparse and rainfall is minimal. However, as the season advances into October and November, a significant reduction in dust levels becomes evident across most parts of the country as depicted in AE levels. This decline is primarily due to the onset of the short rainy season, which is most pronounced in central, western, and southern Kenya. The increased rainfall enhances soil moisture and promotes vegetative growth, both of which inhibit dust uplift by stabilizing the land surface and reducing wind erosion [59].

Lastly, in the months of December (**Figure 3(l)**), dust aerosols dominate over Kenya as depicted by low AE ($AE < 0.7$). This period coincides with the dry season in much of the country, particularly over the northeastern, eastern, and northern arid and semi-arid regions such as Turkana, Marsabit, Isiolo, and Garissa**.** These regions experience minimal rainfall**,** leading to dry and exposed soils that are highly susceptible to wind erosion. The lack of vegetation during this season further exacerbates surface vulnerability, allowing large quantities of dust to be lifted into the atmosphere.

3.1.4. Dust Mass Concentration

The monthly distribution of dust mass concentration over Kenya, as illustrated in **Figure 4**, reveals notable spatial and seasonal variability. The values, represented in micrograms per cubic metre ($\mu g/m^3$), range from 0.01 to 0.10 as indicated on the color scale. The northwestern part of Kenya, particularly the region bordering South Sudan and Uganda, stands out as a persistent dust hotspot throughout the year. This area frequently records the highest concentrations, often exceeding 0.08 $\mu g/m^3$ [9].

The peak dust activity is observed around March (**Figure 4(c)**), where values in the northwestern zone reach the maximum threshold of 0.10 $\mu g/m^3$. This suggests intensified atmospheric dust loading, possibly driven by prevailing dry conditions and strong winds that facilitate the lifting and transport of dust from arid surfaces

such as the Turkana Basin and nearby dry lakebeds.

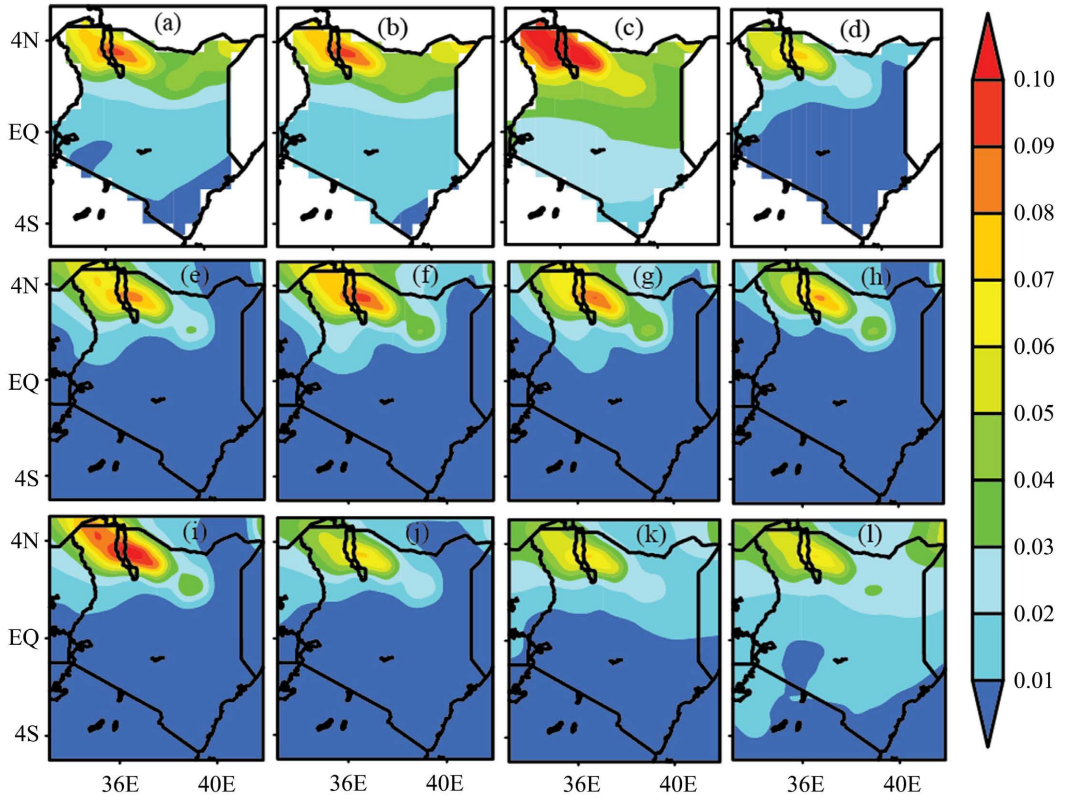

Figure 4. *Monthly spatial distribution of dust mass concentration* (μg/m³) *over Kenya.* Panels (a) to (l) represent specific months from January to December, respectively. The color scale indicates dust mass concentration values ranging from 0.01 μg/m³ to 0.10 μg/m³.

In contrast, the central, southern, and western parts of Kenya consistently show lower dust mass concentrations (<0.03 μg/m³). This is particularly evident during the mid-year months (May to August; **Figures 4(e)-(h)**). During this period, precipitation likely suppresses dust emissions and atmospheric loading by increasing soil moisture and promoting vegetation growth, which acts as a natural barrier to wind erosion.

During the end of the dry season in September and beginning of the short rains that extend into November, dust concentrations begin to rise again, particularly in the northwestern regions. However, these later months (**Figures 4(i)-(k)**) generally exhibit slightly lower peak values (~0.09 μg/m³) than those recorded in the early part of the year. While in December (**Figure 4(l)**) shows a return to the high dust loading over the study domain, suggesting a transitional period before the next cycle of elevated dust begins.

3.1.5. Direct Radiative Forcing of Dust

The radiative forcing due to dust aerosols varies considerably throughout the year, with distinct patterns observed at the top of the atmosphere (TOA), bottom of the atmosphere (BOA), and within the atmospheric (ATM) column (**Table 2**).

Table 2. Monthly Variation of dust-AOD mixing ratio and associated Radiative Forcing (RF) at the Top of Atmosphere (TOA), Bottom of Atmosphere (BOA), and Within the Atmosphere (ATM).

Months	Dust-AOD mixing ratio ($\frac{AOD_{Dust}}{AOD_{Total}}$)	TOTAL RF TOA (W/m^2)	Dust RF TOA (W/m^2)	TOTAL RF BOA (W/m^2)	Dust RF BOA (W/m^2)	Dust RF within ATM (W/m^2)
January	0.2935	−3.213	**−0.943**	−7.379	**−2.165**	**1.223**
February	0.3260	−3.466	**−1.130**	−8.148	**−2.656**	**1.527**
March	0.3506	−3.025	**−1.061**	−7.230	**−2.535**	**1.474**
April	0.2894	−2.027	**−0.587**	−4.609	**−1.334**	**0.747**
May	0.3059	−2.172	**−0.664**	−4.414	**−1.350**	**0.686**
June	0.4449	−3.969	**−1.766**	−8.471	**−3.768**	**2.003**
July	0.3324	−4.158	**−1.382**	−9.913	**−3.295**	**1.913**
August	0.2115	−2.955	**−0.625**	−8.061	**−1.705**	**1.080**
September	0.1865	−2.394	**−0.446**	−7.108	**−1.326**	**0.879**
October	0.1645	−1.995	**−0.328**	−5.813	**−0.956**	**0.628**
November	0.2179	−2.266	**−0.493**	−5.568	**−1.213**	**0.719**
December	0.2577	−2.821	**−0.727**	−6.564	**−1.691**	**0.964**

To start with is the RF at TOA. The dust aerosols predominantly exert a negative radiative forcing, indicating a net cooling effect. This occurs because dust particles scatter incoming solar radiation back to space, thereby reducing the amount of energy absorbed by the Earth system [27]. The strongest cooling at the TOA is observed during June and July, with values of −1.77 W/m^2 and −1.38 W/m^2 respectively. These months also coincide with higher dust-AOD mixing ratios, suggesting more intense dust activity. In contrast, the least cooling occurs in October (−0.33 W/m^2), aligning with the lowest dust-AOD mixing ratio recorded for the year.

At the BOA, dust aerosols also contribute to a significant reduction in solar radiation reaching the Earth's surface, resulting in surface cooling. This effect is most pronounced in June and July, with radiative forcing values of −3.77 W/m^2 and −3.29 W/m^2, respectively. These substantial negative values highlight the capacity of dust to obstruct solar radiation during peak dry seasons, when dust concentrations are typically high due to arid conditions and increased surface winds. Conversely, October shows the lowest magnitude of surface cooling, with a value of −0.96 W/m^2, consistent with lower dust presence.

Within the atmosphere, the difference between TOA and BOA dust RF reveals a positive net forcing, indicating atmospheric heating. This occurs because dust aerosols absorb part of the incoming solar radiation, warming the atmospheric column. The highest atmospheric heating is again observed in June (2.003 W/m^2) and July (1.913 W/m^2), mirroring the pattern seen at the TOA and BOA. The lowest heating effect within the atmosphere is recorded in October (0.628 W/m^2), re-

flecting the minimal dust contribution during this period.

4. Conclusions and Recommendations

4.1. Conclusions

Using multi-year aerosol data sets retrieved from MODIS and the MERRA-2 Model, the present study revealed an in-depth understanding of spatial trends in dust as well as dust radiative forcing over Kenya for the period 2000-2024 and the conclusion drawn from the findings as follows.

1) The monthly dust variation over Kenya is largely governed by seasonal rainfall patterns, wind dynamics and surface characteristics. The highest dust levels occur during the dry months, driven by strong northeasterly winds and dry soil conditions in the north. Dust levels steadily decline with the onset and progression of the rainy seasons, reaching their minimum during September to November when soil moisture and vegetation cover are at their peak. A modest increase in December signals the transition back into the dry season, setting the stage for the next annual dust cycle.

2) On size distribution, the study domain showed a distinct inverse relationship between the size distribution and AOD_{Dust} especially during dust-dominated periods in the JF and JJAS and in arid regions such as northern and northeastern Kenya. High AOD_{Dust} values during these periods indicate large aerosol loads composed mainly of coarse-mode dust particles, which are associated with low AE values (typically <0.6). Conversely, during wetter months or in areas with more vegetation and urban activity. AOD_{Dust} tends to decrease while AE increases due to the greater influence of fine-mode aerosols from biomass burning and anthropogenic sources.

3) The analysis of monthly RF values reveals a clear seasonal variability in the impact of dust aerosols on the Earth's radiation balance. High dust, particularly observed in June and July, corresponds to more negative radiative forcing at both TOA and BOA of the atmosphere, indicating stronger cooling effects due to dust scattering and absorption. Simultaneously, the positive radiative forcing within the atmosphere peaks during these months, suggesting enhanced atmospheric heating from dust absorption. Conversely, lower dust contributions in months like October and September are associated with weaker radiative forcing at all levels.

4.2. Recommendations

Based on the findings on long-term characterization of dust and its radiative forcing over Kenya, the study recommends a strengthened integrated dust monitoring systems that capture both optical and physical characteristics of aerosols across the study domain. Since high Dust AOD and mass concentrations are often observed during dry periods, targeted mitigation measures such as reforestation, windbreaks and sustainable land use should be implemented to reduce surface erosion and dust uplift.

Conflicts of Interest

The authors declare no conflicts of interest regarding the publication of this paper.

References

[1] IPCC (2013) Climate Change 2013: The Physical Science Basis. Contribution of Working Group-I to the Fifth 4 Assessment Report of the Intergovernmental Panel on Climate Change. Cambridge University Press, 1535. https://doi.org/10.1017/CBO9781107415324

[2] Intergovernmental Panel on Climate Change (IPCC) (2023) Climate Change 2021—The Physical Science Basis. Cambridge University Press. https://doi.org/10.1017/9781009157896

[3] Seinfeld, J.H., Pandis, S.N. and Noone, K. (1998) *atmospheric Chemistry and Physics*: *From Air Pollution to Climate Change*. *Physics Today*, **51**, 88-90. https://doi.org/10.1063/1.882420

[4] Tang, R., Lu, Q., Guo, S., Wang, H., Song, K., Yu, Y., *et al.* (2021) Measurement Report: Distinct Emissions and Volatility Distribution of Intermediate-Volatility Organic Compounds from On-Road Chinese Gasoline Vehicles: Implication of High Secondary Organic Aerosol Formation Potential. *Atmospheric Chemistry and Physics*, **21**, 2569-2583. https://doi.org/10.5194/acp-21-2569-2021

[5] Khamala, G.W., Makokha, J.W., Boiyo, R. and Kumar, K.R. (2022) Long-Term Climatology and Spatial Trends of Absorption, Scattering, and Total Aerosol Optical Depths over East Africa during 2001-2019. *Environmental Science and Pollution Research*, **29**, 61283-61297. https://doi.org/10.1007/s11356-022-20022-6

[6] Aloysius, M., Mohan, M., Babu, S.S., Nair, V.S., Parameswaran, K. and Moorthy, K.K. (2008) Influence of Circulation Parameters on the AOD Variations over the Bay of Bengal during ICARB. *Journal of Earth System Science*, **117**, 353-360. https://doi.org/10.1007/s12040-008-0038-6

[7] Deng, X., Cao, W., Huo, Y., Yang, G., Yu, C., He, D., *et al.* (2018) Meteorological Conditions during a Severe, Prolonged Regional Heavy Air Pollution Episode in Eastern China from December 2016 to January 2017. *Theoretical and Applied Climatology*, **135**, 1105-1122. https://doi.org/10.1007/s00704-018-2426-4

[8] Guillén-Lambea, S., Carvalho, M., Delgado, M. and Lazaro, A. (2020) Sustainable Enhancement of District Heating and Cooling Configurations by Combining Thermal Energy Storage and Life Cycle Assessment. *Clean Technologies and Environmental Policy*, **23**, 857-867. https://doi.org/10.1007/s10098-020-01941-9

[9] Khamala, G.W. and Makokha, J.W. (2025) Spatiotemporal Variability and Source Apportionment of Particulate Matter (PM) Emissions Using Binned Size Distributions: Insights from MERRA-2 over Africa. *Earth Systems and Environment*. https://doi.org/10.1007/s41748-025-00641-y

[10] Charlson, R.J., Schwartz, S.E., Hales, J.M., Cess, R.D., Coakley, J.A., Hansen, J.E., *et al.* (1992) Climate Forcing by Anthropogenic Aerosols. *Science*, **255**, 423-430. https://doi.org/10.1126/science.255.5043.423

[11] Ramanathan, V., Crutzen, P.J., Kiehl, J.T. and Rosenfeld, D. (2001) Aerosols, Climate, and the Hydrological Cycle. *Science*, **294**, 2119-2124. https://doi.org/10.1126/science.1064034

[12] Satheesh, S. and Krishnamoorthy, K. (2005) Radiative Effects of Natural Aerosols: A Review. *Atmospheric Environment*, **39**, 2089-2110. https://doi.org/10.1016/j.atmosenv.2004.12.029

[13] Myhre, G. (2009) Consistency between Satellite-Derived and Modeled Estimates of the Direct Aerosol Effect. *Science*, **325**, 187-190. https://doi.org/10.1126/science.1174461

[14] Hansen, J., Sato, M. and Ruedy, R. (1997) Radiative Forcing and Climate Response. *Journal of Geophysical Research*: *Atmospheres*, **102**, 6831-6864. https://doi.org/10.1029/96jd03436

[15] Lee, K.H., Li, Z., Wong, M.S., Xin, J., Wang, Y., Hao, W., *et al.* (2007) Aerosol Single Scattering Albedo Estimated across China from a Combination of Ground and Satellite Measurements. *Journal of Geophysical Research*: *Atmospheres*, **112**, D22S15. https://doi.org/10.1029/2007jd009077

[16] Bahino, J., Giordano, M., Beekmann, M., Yoboué, V., Ochou, A., Galy-Lacaux, C., *et al.* (2024) Temporal Variability and Regional Influences of $PM_{2.5}$ in the West African Cities of Abidjan (Côte d'Ivoire) and Accra (Ghana). *Environmental Science*: *Atmospheres*, **4**, 468-487. https://doi.org/10.1039/d4ea00012a

[17] Sokolik, I.N. and Toon, O.B. (1999) Incorporation of Mineralogical Composition into Models of the Radiative Properties of Mineral Aerosol from UV to IR Wavelengths. *Journal of Geophysical Research*: *Atmospheres*, **104**, 9423-9444. https://doi.org/10.1029/1998jd200048

[18] Lyamani, H., Olmo, F.J. and Alados-Arboledas, L. (2009) Physical and Optical Properties of Aerosols over an Urban Location in Spain: Seasonal and Diurnal Variability. *Atmospheric Chemistry and Physics*, **9**, 18159-18199. https://doi.org/10.5194/acpd-9-18159-2009

[19] El-Metwally, M., Alfaro, S.C., Wahab, M.M.A., Favez, O., Mohamed, Z. and Chatenet, B. (2011) Aerosol Properties and Associated Radiative Effects over Cairo (Egypt). *Atmospheric Research*, **99**, 263-276. https://doi.org/10.1016/j.atmosres.2010.10.017

[20] Makokha, J.W. and Angeyo, H.K. (2013) Investigation of Radiative Characteristics of the Kenyan Atmosphere Due to Aerosols Using Sun Spectrophotometry Measurements and the COART Model. *Aerosol and Air Quality Research*, **13**, 201-208. https://doi.org/10.4209/aaqr.2012.06.0146

[21] Esteve, A.R., Estellés, V., Utrillas, M.P. and Martínez-Lozano, J.A. (2014) Analysis of the Aerosol Radiative Forcing over a Mediterranean Urban Coastal Site. *Atmospheric Research*, **137**, 195-204. https://doi.org/10.1016/j.atmosres.2013.10.009

[22] Kumar, S., Dey, S. and Srivastava, A. (2016) Quantifying Enhancement in Aerosol Radiative Forcing during "Extreme Aerosol Days" in Summer at Delhi National Capital Region, India. *Science of the Total Environment*, **550**, 994-1000. https://doi.org/10.1016/j.scitotenv.2016.01.191

[23] Kumar, K.R., Kang, N., Sivakumar, V. and Griffith, D. (2017) Temporal Characteristics of Columnar Aerosol Optical Properties and Radiative Forcing (2011-2015) Measured at AERONET's Pretoria_CSIR_DPSS Site in South Africa. *Atmospheric Environment*, **165**, 274-289. https://doi.org/10.1016/j.atmosenv.2017.06.048

[24] Bibi, H., Alam, K., Blaschke, T., Bibi, S. and Iqbal, M.J. (2016) Long-Term (2007-2013) Analysis of Aerosol Optical Properties over Four Locations in the Indo-Gangetic Plains. *Applied Optics*, **55**, 6199. https://doi.org/10.1364/ao.55.006199

[25] Adesina, A.J., Kumar, K.R., Sivakumar, V. and Piketh, S.J. (2016) Intercomparison and Assessment of Long-Term (2004-2013) Multiple Satellite Aerosol Products over Two Contrasting Sites in South Africa. *Journal of Atmospheric and Solar-Terrestrial Physics*, **148**, 82-95. https://doi.org/10.1016/j.jastp.2016.09.001

[26] Khan, R., Kumar, K.R., Zhao, T. and Ali, G. (2020) The Contribution of Different Aerosol Types to Direct Radiative Forcing over Distinct Environments of Pakistan

Inferred from the AERONET Data. *Environmental Research Letters*, **15**, Article ID: 114062. https://doi.org/10.1088/1748-9326/aba2a6

[27] Khamala, G.W., Makokha, J.W., Boiyo, R. and Kumar, K.R. (2023) Spatiotemporal Analysis of Absorbing Aerosols and Radiative Forcing over Environmentally Distinct Stations in East Africa during 2001-2018. *Science of the Total Environment*, **864**, Article ID: 161041. https://doi.org/10.1016/j.scitotenv.2022.161041

[28] Gauderman, W.J., Gilliland, G.F., Vora, H., Avol, E., Stram, D., McConnell, R., *et al.* (2002) Association between Air Pollution and Lung Function Growth in Southern California Children: Results from a Second Cohort. *American Journal of Respiratory and Critical Care Medicine*, **166**, 76-84. https://doi.org/10.1164/rccm.2111021

[29] Liao, W., Wang, X., Fan, Q., Zhou, S., Chang, M., Wang, Z., *et al.* (2015) Long-term Atmospheric Visibility, Sunshine Duration and Precipitation Trends in South China. *Atmospheric Environment*, **107**, 204-216. https://doi.org/10.1016/j.atmosenv.2015.02.015

[30] Yu, X., Kumar, K.R., Lü, R. and Ma, J. (2016) Changes in Column Aerosol Optical Properties during Extreme Haze-Fog Episodes in January 2013 over Urban Beijing. *Environmental Pollution*, **210**, 217-226. https://doi.org/10.1016/j.envpol.2015.12.021

[31] Mahowald, N., Albani, S., Kok, J.F., Engelstaeder, S., Scanza, R., Ward, D.S., *et al.* (2014) The Size Distribution of Desert Dust Aerosols and Its Impact on the Earth System. *Aeolian Research*, **15**, 53-71. https://doi.org/10.1016/j.aeolia.2013.09.002

[32] Jickells, T.D., An, Z.S., Andersen, K.K., Baker, A.R., Bergametti, G., Brooks, N., *et al.* (2005) Global Iron Connections between Desert Dust, Ocean Biogeochemistry, and Climate. *Science*, **308**, 67-71. https://doi.org/10.1126/science.1105959

[33] Wu, W., Purser, R.J. and Parrish, D.F. (2002) Three-Dimensional Variational Analysis with Spatially Inhomogeneous Covariances. *Monthly Weather Review*, **130**, 2905-2916. https://doi.org/10.1175/1520-0493(2002)130<2905:tdvaws>2.0.co;2

[34] Rienecker, M.M., Suarez, M.J., Gelaro, R., Todling, R., Bacmeister, J., Liu, E., *et al.* (2011) MERRA: Nasa's Modern-Era Retrospective Analysis for Research and Applications. *Journal of Climate*, **24**, 3624-3648. https://doi.org/10.1175/jcli-d-11-00015.1

[35] Remer, L.A., Kaufman, Y.J., Tanré, D., Mattoo, S., Chu, D.A., Martins, J.V., *et al.* (2005) The MODIS Aerosol Algorithm, Products, and Validation. *Journal of the Atmospheric Sciences*, **62**, 947-973. https://doi.org/10.1175/jas3385.1

[36] Gelaro, R., McCarty, W., Suárez, M.J., Todling, R., Molod, A., Takacs, L., *et al.* (2017) The Modern-Era Retrospective Analysis for Research and Applications, Version 2 (MERRA-2). *Journal of Climate*, **30**, 5419-5454. https://doi.org/10.1175/jcli-d-16-0758.1

[37] Kok, J.F., Ward, D.S., Mahowald, N.M. and Evan, A.T. (2012) Global and Regional Importance of the Direct Dust-Climate Feedback. *Nature Climate Change*, **2**, 437-445.

[38] Ginoux, P., Prospero, J.M., Gill, T.E., Hsu, N.C. and Zhao, M. (2012) Global-Scale Attribution of Anthropogenic and Natural Dust Sources and Their Emission Rates Based on MODIS Deep Blue Aerosol Products. *Reviews of Geophysics*, **50**, RG3005. https://doi.org/10.1029/2012rg000388

[39] Eck, T.F., Holben, B.N., Reid, J.S., Arola, A., Ferrare, R.A., Hostetler, C.A., Sinyuk, A., *et al.* (2013) High Aerosol Absorption Optical Depths from Biomass Burning over the Southeast United States during the Summer of 2007: An Analysis Using Surface and Satellite Measurements. *Journal of Geophysical Research*: *Atmospheres*, **118**, 12-205.

[40] Evan, A.T., Flamant, C., Gaetani, M. and Guichard, F. (2016) The Past, Present and

Future of African Dust. *Science Advances*, **2**, e1500646.

[41] Chatoutsidou, S.E., Diapouli, E., Manousakas, M., Vratolis, S., Maggos, T. and Eleftheriadis, K. (2019) Assessment of PM_{10}-Bound Heavy Metals Seasonal Variation and Health Impact in Two Low Pollution Areas of Greece. *Air Quality, Atmosphere & Health*, **12**, 547-558.

[42] Gahungu, P., Kubwimana, J.R., Muhimpundu, L.J.M.B. AND Ndamuzi, E. (2022) Modelling Spatio-Temporal Trends of Air Pollution in Africa: A Case Study of $PM_{2.5}$ Variations across Different Regions. arXiv: 2208.12719.

[43] Kalisa, E., Clark, M.L., Ntakirutimana, T., Amani, M. and Volckens, J. (2023) Exposure to Indoor and Outdoor Air Pollution in Schools in Africa: Current Status, Knowledge Gaps, and a Call to Action. *Heliyon*, **9**, e18450. https://doi.org/10.1016/j.heliyon.2023.e18450

[44] Mugagga, F., Nakanjakko, N., Nakileza, B. and Nseka, D. (2020) Vulnerability of Smallholder Sorghum Farmers to Climate Variability in a Heterogeneous Landscape of South-Western Uganda. *Jàmbá Journal of Disaster Risk Studies*, **12**, a849. https://doi.org/10.4102/jamba.v12i1.849

[45] Mutama, P.M., Makokha, J.W., Kelonye, F.B. and Khamala, G.W. (2024) Spatial-Temporal Assessment of Changes in Aerosol Optical Properties Pre, During, and Post COVID-19 Lockdowns over Kenya, East Africa. *Open Access Library Journal*, **11**, e11223. https://doi.org/10.4236/oalib.1111223

[46] Ngaina, J., Mutai, B., Ininda, J. and Muthama, J. (2014) Monitoring Spatial-Temporal Variability of Aerosol over Kenya. *Ethiopian Journal of Environmental Studies and Management*, **7**, 244-252. https://doi.org/10.4314/ejesm.v7i3.3

[47] Ongoma, V. and Chen, H. (2016) Temporal and Spatial Variability of Temperature and Precipitation over East Africa from 1951 to 2010. *Meteorology and Atmospheric Physics*, **129**, 131-144. https://doi.org/10.1007/s00703-016-0462-0

[48] Makokha, J.W., Odhiambo, J.O. and Shem, J.G. (2018) Long Term Assessment of Aerosol Radiative Forcing over Selected Sites of East Africa. *Journal of Geoscience and Environment Protection*, **6**, 22-34. https://doi.org/10.4236/gep.2018.64002

[49] Boiyo, R., Kumar, K.R. and Zhao, T. (2018) Spatial Variations and Trends in AOD Climatology over East Africa during 2002-2016: A Comparative Study Using Three Satellite Data Sets. *International Journal of Climatology*, **38**, e1221-e1240. https://doi.org/10.1002/joc.5446

[50] Kaufman, Y.J., Koren, I., Remer, L.A., Rosenfeld, D. and Rudich, Y. (2005) The Effect of Smoke, Dust, and Pollution Aerosol on Shallow Cloud Development over the Atlantic Ocean. *Proceedings of the National Academy of Sciences of the United States of America*, **102**, 11207-11212. https://doi.org/10.1073/pnas.0505191102

[51] Hsu, N.C., Jeong, M.-., Bettenhausen, C., Sayer, A.M., Hansell, R., Seftor, C.S., *et al.* (2013) Enhanced Deep Blue Aerosol Retrieval Algorithm: The Second Generation. *Journal of Geophysical Research*: *Atmospheres*, **118**, 9296-9315. https://doi.org/10.1002/jgrd.50712

[52] Sayer, A.M., Hsu, N.C., Bettenhausen, C. and Jeong, M. (2013) Validation and Uncertainty Estimates for MODIS Collection 6 "Deep Blue" Aerosol Data. *Journal of Geophysical Research*: *Atmospheres*, **118**, 7864-7872. https://doi.org/10.1002/jgrd.50600

[53] Sayer, A.M., Munchak, L.A., Hsu, N.C., Levy, R.C., Bettenhausen, C. and Jeong, M. (2014) MODIS Collection 6 Aerosol Products: Comparison between Aqua's E-Deep Blue, Dark Target, and "Merged" Data Sets, and Usage Recommendations. *Journal of Geophysical Research*: *Atmospheres*, **119**, 13965-13989.

https://doi.org/10.1002/2014jd022453

[54] Levy, R.C., Remer, L.A., Kleidman, R.G., Mattoo, S., Ichoku, C., Kahn, R., *et al.* (2010) Global Evaluation of the Collection 5 MODIS Dark-Target Aerosol Products over Land. *Atmospheric Chemistry and Physics*, **10**, 10399-10420. https://doi.org/10.5194/acp-10-10399-2010

[55] Smirnov, A., Holben, B.N., Eck, T.F., Slutsker, I., Chatenet, B. and Pinker, R.T. (2000) Aerosol Optical Depth Measurements during the Aerosols99 Experiment. *Journal of Geophysical Research*: *Atmospheres*, **105**, 15127-15138.

[56] Eck, T.F., Holben, B.N., Sinyuk, A., Pinker, R.T., Goloub, P., Chen, H., *et al.* (2010) Climatological Aspects of the Optical Properties of Fine/Coarse Mode Aerosol Mixtures. *Journal of Geophysical Research*: *Atmospheres*, **115**, D19205. https://doi.org/10.1029/2010jd014002

[57] Khamala, G.W., Odhiambo, J.O. and Makokha, J.W. (2018) Seasonal Variability in Aerosol Microphysical Properties over Selected Rural, Urban and Maritime Sites in Kenya. *Open Access Library Journal*, **5**, e4821. https://doi.org/10.4236/oalib.1104821

[58] Miller, R.L., Tegen, I. and Perlwitz, J. (2004) Surface Radiative Forcing by Soil Dust Aerosols and the Hydrologic Cycle. *Journal of Geophysical Research*: *Atmospheres*, **109**, D04203. https://doi.org/10.1029/2003jd004085

[59] Makokha, J., Masayi, N., Barasa, P., Ikoha, P., Konje, M., Mutonyi, J., *et al.* (2024) Assessing the Long-Term Changes in Selected Meteorological Parameters over the North-Rift, Kenya: A Regional Climatology Perspective. *Hydrology*, **12**, 59-76. https://doi.org/10.11648/j.hyd.20241203.12

[60] Khamala, G.W., Makokha, J.W. and Boiyo, R. (2024) The Spatiotemporal and Dependency Analysis of Selected Meteorological Parameters and Normalized Difference Vegetation Index with Aerosol Optical Depth over East Africa. *Heliyon*, **10**, e39961. https://doi.org/10.1016/j.heliyon.2024.e39961